Latent light-assisted poling of $LiNbO_3$

Y. J. Ying,[1,*] C. E. Valdivia,[1,2] C. L. Sones,[1] R. W. Eason[1] and S. Mailis[1]

[1]*Optoelectronics Research Centre, University of Southampton, Southampton, S017 1BJ, UK*
[2]*Centre for Research in Photonics, University of Ottawa, Ottawa, K1N 6N5, Canada*
**yoy@orc.soton.ac.uk*

Abstract: The observation of latent light-assisted poling (LAP) in lithium niobate single crystals is reported. More specifically, the nucleation field is reduced and remains reduced for an extended time period (up to several hours) after irradiation with ultrafast (~150 fs) laser light at a wavelength of 400 nm. The maximum nucleation field reduction measured using latent-LAP (62%) was significantly higher in comparison with regular non-time-delayed LAP (41%) under identical irradiation conditions in undoped congruent lithium niobate crystals. No latent-LAP effect was observed in MgO-doped crystals for the experimental conditions used, despite the strong effect observed using regular LAP. The latent-LAP effect is attributed to the formation of a slowly decaying photo-induced space-charge distribution which assists local ferroelectric domain nucleation. The dynamics of latent-LAP are compared with the dynamics of photorefractive grating decay, recorded in lithium niobate crystals of different doping, confirming the space charge hypothesis.

©2009 Optical Society of America

OCIS codes: (140.3538) Lasers, pulsed; (160.5320) Photorefractive materials; (160.2260) Ferroelectrics; (160.3730) Lithium niobate; (090.5694) Real-time holography.

References and links

1. L. Arizmendi, "Photonic applications of lithium niobate crystals," Phys. Status Solidi A **201**, 253–283 (2004). *http://dx.doi.org/10.1002/pssa.200303911*
2. I. E. Barry, G. W. Ross, P. G. R. Smith, R. W. Eason, and G. Cook, "Microstructuring of lithium niobate using differential etch-rate between inverted and non-inverted ferroelectric domains," Mater. Lett. **37**(4-5), 246–254 (1998), http://dx.doi.org/10.1016/S0167-577X(98)00100-1.
3. A. J. Boyland, S. Mailis, J. M. Hendricks, P. G. R. Smith, and R. W. Eason, "Electro-optically controlled beam switching via total internal reflection at a domain-engineered interface in $LiNbO_3$," Opt. Commun. **197**(1-3), 193–200 (2001), http://dx.doi.org/10.1016/S0030-4018(01)01428-6.
4. R. W. Eason, A. J. Boyland, S. Mailis, and P. G. R. Smith, "Electro-optically controlled beam deflection for grazing incidence geometry on a domain-engineered interface in $LiNbO_3$," Opt. Commun. **197**(1-3), 201–207 (2001), http://dx.doi.org/10.1016/S0030-4018(01)01429-8.
5. M. Yamada, N. Nada, M. Saitoh, and K. Watanabe, "First-order quasi-phase matched $LiNbO_3$ waveguide periodically poled by applying an external field for efficient blue second-harmonic generation," Appl. Phys. Lett. **62**(5), 435–436 (1993), http://link.aip.org/link/?APL/62/435/1.
6. M. Yamada, and M. Saitoh, "Fabrication of a periodically poled laminar domain structure with a pitch of a few micrometers by applying an external electric field," J. Appl. Phys. **84**(4), 2199–2206 (1998), http://link.aip.org/link/?JAP/84/2199/1.
7. W. Wang, Y. Kong, H. Liu, Q. Hu, S. Liu, S. Chen, and J. Xu, "Light-induced domain reversal in doped lithium niobate crystals," J. Appl. Phys. **105**(4), 043105 (2009), http://dx.doi.org/10.1063/1.3079478.
8. H. Steigerwald, F. Luedtke, and K. Buse, "Ultraviolet light assisted periodic poling of near-stoichiometric, magnesium-doped lithium niobate crystals," Appl. Phys. Lett. **94**(3), 032906 (2009), http://link.aip.org/link/?APL/94/032906/1.
9. M. Fujimura, T. Sohmura, and T. Suhara, "Fabrication of domain-inverted gratings in $MgO:LiNbO_3$ by applying voltage under ultraviolet irradiation through photomask at room temperature," Electron. Lett. **39**(9), 719–721 (2003), http://ieeexplore.ieee.org/xpls/abs_all.jsp?isnumber=27015&arnumber=1199952&count=36&index=12.
10. C. L. Sones, M. C. Wengler, C. E. Valdivia, S. Mailis, R. W. Eason, and K. Buse, "Light-induced order-of-magnitude decrease in the electric field for domain nucleation in MgO-doped lithium niobate crystals," Appl. Phys. Lett. **86**(21), 212901 (2005), http://link.aip.org/link/?APL/86/212901/1.
11. V. Dierolf, and C. Sandmann, "Direct-write method for domain inversion patterns in $LiNbO_3$," Appl. Phys. Lett. **84**(20), 3987–3989 (2004), http://link.aip.org/link/?APL/84/3987/1.

#113891 - $15.00 USD Received 7 Jul 2009; revised 20 Aug 2009; accepted 23 Aug 2009; published 1 Oct 2009
(C) 2009 OSA

12. M. C. Wengler, B. Fassbender, E. Soergel, and K. Buse, "Impact of ultraviolet light on coercive field, poling dynamics and poling quality of various lithium niobate crystals from different sources," J. Appl. Phys. **96**(5), 2816–2820 (2004), http://link.aip.org/link/?JAP/96/2816/1.
13. C. E. Valdivia, C. L. Sones, S. Mailis, J. D. Mills, and R. W. Eason, "Ultrashort-pulse optically-assisted domain engineering in lithium niobate," Ferroelectrics **340**(1), 75–82 (2006), http://www.informaworld.com/10.1080/00150190600888983.
14. J. H. Ro, and M. Cha, "Subsecond relaxation of internal field after polarization reversal in congruent $LiNbO_3$ and $LiTaO_3$ crystals," Appl. Phys. Lett. **77**(15), 2391–2393 (2000), http://link.aip.org/link/?APL/77/2391/1.
15. A. I. Lobov, V. Y. Shur, I. S. Baturin, E. I. Shishkin, D. K. Kuznetsov, A. G. Shur, M. A. Dolbilov, and K. Gallo, "Field induced evolution of regular and random 2D domain structures and shape of isolated domains in $LiNbO_3$ and $LiTaO_3$," Ferroelectrics **341**(1), 109–116 (2006), http://www.informaworld.com/smpp/content~db=all~content=a769409747~tab=content.
16. Ya. Vladimir, Shur, "Correlated Nucleation and Self-Organized Kinetics of Ferroelectric Domains," in *Nucleation Theory and Applications*, W. P. S. Dr. Jürn, ed. (2005), pp. 178–214. *http://dx.doi.org/10.1002/3527604790.ch6*
17. W. Yan, L. Shi, Y. Kong, Y. Wang, H. Liu, J. Xu, S. Chen, L. Zhang, Z. Huang, S. Liu, and G. Zhang, "The electrostatic depinning mechanism of domain wall for near-stoichiometric lithium niobate crystals," J. Phys. D Appl. Phys. **39**(19), 4245–4249 (2006), http://www.iop.org/EJ/abstract/0022-3727/39/19/018.
18. B. Sturman, M. Carrascosa, and F. Agulló-López, "Light-induced charge transport in $LiNbO_3$ crystals," Phys. Rev. B **78**(24), 245114 (2008), http://link.aps.org/doi/10.1103/PhysRevB.78.245114.
19. O. Beyer, D. Maxein, K. Buse, B. Sturman, H. T. Hsieh, and D. Psaltis, "Femtosecond time-resolved absorption processes in lithium niobate crystals," Opt. Lett. **30**(11), 1366–1368 (2005), http://ol.osa.org/abstract.cfm?URI=ol-30-11-1366.
20. L. Arizmendi, and F. Agulló-López, "$LiNbO_3$: A paradigm for photorefractive materials," MRS Bull. **19**, 32–38 (1994).
21. F. H. Mok, "Angle-multiplexed storage of 5000 holograms in lithium niobate," Opt. Lett. **18**(11), 915–917 (1993), http://www.opticsinfobase.org/abstract.cfm?URI=ol-18-11-915.
22. Y. S. Bai, and R. Kachru, "Nonvolatile holographic storage with two-step recording in lithium niobate using cw lasers," Phys. Rev. Lett. **78**(15), 2944–2947 (1997), http://prola.aps.org/abstract/PRL/v78/i15/p2944_1.
23. F. Jermann, M. Simon, and E. Krätzig, "Photorefractive properties of congruent and stoichiometric lithium niobate at high light intensities," J. Opt. Soc. Am. B **12**(11), 2066–2070 (1995), http://josab.osa.org/abstract.cfm?URI=josab-12-11-2066.
24. D. Berben, K. Buse, S. Wevering, P. Herth, M. Imlau, and T. Woike, "Lifetime of small polarons in iron-doped lithium–niobate crystals," J. Appl. Phys. **87**(3), 1034–1041 (2000), http://link.aip.org/link/?JAP/87/1034/1.
25. K. Mizuuchi, A. Morikawa, T. Sugita, and K. Yamamoto, "Polarisation-switching-induced resistance change in ferroelectric Mg-doped $LiNbO_3$ single crystals," Electron. Lett. **40**(13), 819–820 (2004), http://ieeexplore.ieee.org/xpls/abs_all.jsp?arnumber=1309740.
26. I. Nee, M. Müller, K. Buse, and E. Krätzig, "Role of iron in lithium-niobate crystals for the dark-storage time of holograms," J. Appl. Phys. **88**(7), 4282–4286 (2000), http://link.aip.org/link/?JAP/88/4282/1.
27. A. Mansingh, and A. Dhar, "The AC conductivity and dielectric constant of lithium niobate single crystals," J. Phys. D Appl. Phys. **18**(10), 2059–2071 (1985), http://www.iop.org/EJ/abstract/0022-3727/18/10/016.
28. R. T. Smith, and F. S. Welsh, "Temperature dependence of the elastic, piezoelectric, and dielectric constants of lithium tantalate and lithium niobate," J. Appl. Phys. **42**(6), 2219–2230 (1971), http://link.aip.org/link/?JAPIAU/42/2219/1.
29. C. E. Valdivia, "Light-induced ferroelectric domain engineering in lithium niobate & lithium tantalate," (PhD thesis, University of Southampton, Southampton, 2007). *http://www.orc.soton.ac.uk/viewpublication.html?pid=3846*

1. Introduction

Single crystal lithium niobate (LN) is a ferroelectric crystal, which exhibits a spontaneous electric polarization along its z-axis, the direction of which can be inverted by the application of an external electric field (*E*-field). Ferroelectric domain engineering of LN has received much interest for applications in nonlinear frequency conversion, electro-optic modulation [1], surface micro-structuring [2], beam switching [3], and deflection [4].

The most common domain engineering technique for LN is electric field poling (EFP), where a photolithographically-patterned electrode provides a spatially modulated *E*-field across the crystal in the z-axis [5,6]. Recent research investigating the influence of light on EFP revealed that illuminated regions require a lower nucleation field, E_n (the *E*-field required for microscopic ferroelectric domain nucleation) in both undoped congruent LN (CLN) and MgO-doped LN using c.w. [7–12] and pulsed laser light [13] in a process referred to as *light-assisted poling* (LAP). Utilizing ultrafast lasers at wavelengths ranging between 305 nm and 800 nm, LAP has been observed to produce significant E_n reductions, of up to two orders of magnitude for MgO:CLN [13].

#113891 - $15.00 USD Received 7 Jul 2009; revised 20 Aug 2009; accepted 23 Aug 2009; published 1 Oct 2009
(C) 2009 OSA

In all cases of LAP reported thus far, the light illumination was concurrent with the application of the external *E*-field. In this paper we show that in undoped CLN, the E_n reduction can be observed even several hours after light illumination. Using this technique, called *latent light-assisted poling* (LLAP), the two processes of light illumination and application of an external *E*-field can be de-coupled. Interestingly, the E_n reduction in LLAP (62%) is larger compared to that measured in simultaneous LAP (42%) [13]. The latent effect has not been observed in MgO:CLN for the time scales employed in the experiments here. The dependence of LAP and LLAP on the doping suggests a space-charge-related mechanism. The low dark conductivity in the undoped CLN allows a photo-induced space-charge distribution to persist for a significant period of time after its formation, while in the MgO:CLN any photo-induced space-charge distribution decays much faster due to the much higher dark conductivity which makes this crystal less susceptible to the photorefractive damage. The presence of a photo-induced space-charge distribution and the corresponding space-charge field induces a refractive index change in LN via the electro-optic effect. Probing of this photorefractive index change provides an excellent tool for the investigation of the LLAP dynamics. Therefore, the domain nucleation for varying time-delays between light illumination and application of the external *E*-field in undoped CLN is investigated in Section 2, while in Section 3 the LLAP dynamics are compared to the decay of a photorefractive grating formed by the space-charge field.

2. Latent-LAP

To investigate the process of LLAP, 0.5-mm thick, z-cut, optical grade, undoped CLN crystals (Crystal Technology, Inc.) were held within a transparent cell which enabled the simultaneous light illumination of the crystal and the application of an external *E*-field. This arrangement has been used for previous LAP experiments and a detailed description can be found in [10]. The crystal was subjected to a sequence of processing steps as follows. First, the crystal was domain-inverted three times sequentially, leaving it with a domain orientation anti-parallel to its virgin state. This was done to condition the crystal in order to avoid the first poling cycle which is known to have a higher coercive field [14] and exhibit erratic domain expansion as compared to subsequent poling cycles. Second, a pulsed laser beam (~150 fs, 250 kHz, λ = 400 nm) with a Gaussian intensity profile was focused onto the –z face (front surface) to a spot diameter of ~30 μm for an illumination time of 30 s. The crystal was then repositioned and a new spot was illuminated with identical conditions after a subsequent delay of 30 s. The process was repeated to systematically illuminate a number of spots at precisely controlled times. Third, following the last spot and a final 30 s delay, the voltage was ramped up to the desired value over a period of 30 s, whereupon the maximum voltage was maintained for 300 s, and then ramped back down to 0 V over a final period of 30 s. The *voltage delay time* for each spot is defined as the elapsed time from the end of its illumination to the end of the first voltage ramp. Thus, each spot corresponded to different values of voltage delay time. For the *E*-field step, liquid electrodes were introduced, uniformly covering both crystal faces. The illumination times, time delays and *E*-field application duration were chosen to demonstrate the effect and were not necessarily the optimal experimental conditions. After the above procedure, the samples were briefly etched in hydrofluoric (HF) acid to reveal the preferentially inverted ferroelectric LLAP domains. The area of these inverted domains, measured from scanning electron microscopy (SEM) images, was investigated as a function of the voltage delay time for different laser intensities and *E*-fields.

The inverted LLAP domains formed under all of these exposure conditions were of limited depth, and hence did not extend to the opposite crystal face. However, LLAP domains have been pushed through to the opposite face of the crystal by using higher magnitude of the *E*-field or longer *E*-field application times or a combination of the two. It is important to note that under the process of LLAP, domain inversion occurred only at the locations where the crystal had been previously illuminated. As with regular (simultaneous) LAP, LLAP also formed domains which followed the shape of the illuminating spot and were reproducible

#113891 - $15.00 USD Received 7 Jul 2009; revised 20 Aug 2009; accepted 23 Aug 2009; published 1 Oct 2009
(C) 2009 OSA

between different spots and samples. Etching of the –z face of LN crystal in HF acid reveals the inverted ferroelectric LLAP domains with unetched + z faces as shown in Fig. 1. The LLAP conditions for these particular inverted domains were: laser intensity of 9 GW/cm^2, applied *E*-fields of (a) 14 kV/mm and (b) 8 kV/mm, and voltage time delay of 570 s . As shown in Fig. 1, the LLAP domain walls of (a) follow the crystal symmetry due to the high *E*-field applied which allowed expansion of this domain beyond the confines of the illuminating laser spot area. However, the domain did not form a regular hexagon as is typical for EFP domains, forming instead an irregular octagon with domain walls parallel to both the y- and x-axes. The walls labeled 1, 2, 4, 5, 7, 8 are parallel to y-axes, while walls labeled 3, 6 are parallel to x-axes, contrary to the regular domain wall growth in CLN [15]. The LLAP domain walls of (b) also run parallel to both y- and x-axes, in addition to many more rounded segments, generally following the shape of illumination much more closely due to the lower applied *E*-field. Domain walls following the x-axis imply a condition of incomplete screening of the depolarization field [16], likely a result of the redistribution of the photo-induced space charges prior to application of the external *E*-field.

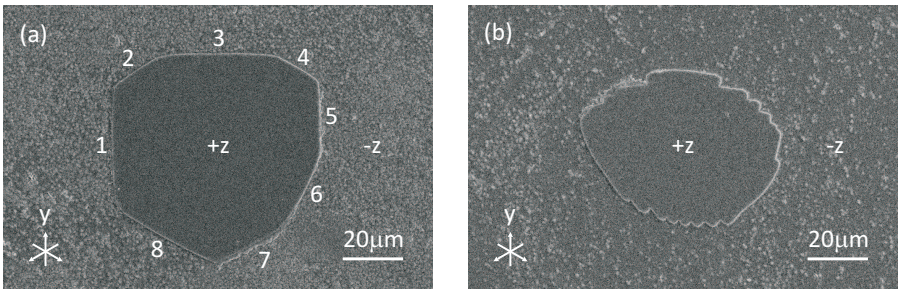

Fig. 1. Preferentially inverted ferroelectric LLAP domains, revealed as unetched + z face after HF etching, are induced by I = 9 GW/cm^2 of 400 nm fs-laser irradiation, followed by applied *E*-fields of (a) 14 kV/mm and (b) 8 kV/mm after a voltage delay time of 570 s in undoped CLN. LLAP domain walls run parallel to both y- and x-axes, particularly for the higher *E*-field in (a).

The nucleation and growth of LLAP domains was investigated by varying the illumination intensity and the applied *E*-field for a series of spots. Figure 2 shows plots of the square root of the inverted LLAP domain areas as a function of voltage delay time for different applied *E*-fields (Fig. 2a) and laser intensities (Fig. 2b). The square root of the inverted domain area is presented here rather than the area itself because it represents the evolution of one linear dimension (1D) of the inverted domain and can be compared in a straightforward manner with the temporal evolution of a 1D space-charge distribution, discussed in Section 3. Figure 2 reveals that, for all exposure conditions, the poled area increases with decreasing voltage delay time. It is expected that at shorter voltage delay times than those applied in the experiments, the poled areas will increase. Our experimental protocol however, limits the shortest applicable voltage delay time to 60 s. Additionally, the poled area increases with increasing laser intensity or *E*-field amplitude. Of particular interest is that domain inversion was observed even for an *E*-field as low as 6 kV/mm (Fig. 2a), a reduction of 62% from the dark E_n (15.8 kV/mm in the reverse poling direction). This is a surprising result as the minimum intensity-dependent E_n observed with simultaneous illumination showed a reduction of only 41% in LAP experiments, as reported in Ref [13], using the same experimental setup. Nevertheless, LLAP formed a sizeable domain even when 6 kV/mm was applied nearly 700 s after illumination. An *E*-field of 6 kV/mm is not necessarily the minimum amplitude to achieve LLAP, but rather represents the minimum value tested under these exposure conditions. The straight lines which appear in Fig. 2a and Fig. 2b corresponds to single exponential decay functions, fitted to the square root of the inverted domain area data points as,

#113891 - $15.00 USD Received 7 Jul 2009; revised 20 Aug 2009; accepted 23 Aug 2009; published 1 Oct 2009
(C) 2009 OSA

$$A^{1/2} = L_0 \exp\left(-t / \tau_L\right) \quad (1)$$

where A is the LLAP inverted domain area, L_0 is a constant and τ_L is the time constant of the 1-D length reduction. The results of the fittings are listed in Table 1. The close values of decay rate (τ_L^{-1}) show that the length-reduction of the inverted domains with voltage delay time is very similar despite of the very diverse experimental conditions in both laser exposure and value of applied E-field. Any differences should be attributed to the uncertainty due to the short range fitting (~10% in Table 1), the stochastic nature of ferroelectric domain nucleation and expansion, and the presence of local defects in the crystal which also govern domain nucleation and growth during regular EFP [17] rather than the exposure and poling conditions. For more accurate measurements, it is necessary to average over many exposure locations as the local crystal quality appears to have a noticeable impact on the growth of LLAP domains. It should be noted here that actually a more reasonable fitting is by a stretched exponential decay instead of a single-exponential decay considering the tunneling-involved charge migration at shallow energy levels [18]. However, the short measurement range and the limited number of data points can induce a significant uncertainty in the fitting of a stretched exponential decay function. Fitting a single exponential function is acceptable however for this short range of time delays (60 s – 720 s). A parameter $\Delta A^{1/2}$, defined as the relative reduction of $A^{1/2}$ from 60 s to 720 s, expressed as

$$\Delta A^{1/2} = 1 - A^{1/2}_{t=720s} \,/\, A^{1/2}_{t=60s} \quad (2)$$

can be used for comparison with the photorefractive grating decay in Section 3. The $\Delta A^{1/2}$ values for each point in Fig. 2 are derived from the single exponential fitting and are listed in Table 1.

Table 1. Summary of constants L_0, time constants τ_L, decay rates τ_L^{-1} and the relative reductions $\Delta A^{1/2}$ from 60 s to 720 s of the linear dimension of the LLAP inverted domains in undoped CLN for different experimental conditions.

E (kV/mm)	I (GW/cm^2)	L_0 (μm)	τ_L (s)	τ_L^{-1} (× 10^{-4} s^{-1})	$\Delta A^{1/2}$
8	4.5	42.4	2860 ± 120	3.50 ± 0.29	0.206
8	9	47.3	3970 ± 470	2.52 ± 0.61	0.153
8	18	54.8	4050 ± 250	2.47 ± 0.31	0.150
14	9	60.8	3010 ± 450	3.33 ± 1.02	0.197
10	9	47.5	2750 ± 250	3.64 ± 0.67	0.213
6	9	35.5	3150 ± 390	3.17 ± 0.80	0.189

Also, Fig. 3 shows that for an E-field (8 kV/mm) or intensity (9 GW/cm^2), the square root of the inverted domain area linearly increases with the intensity or the E-field within that range. The larger slope of the data for constant intensity indicates that the domain area is more sensitive to the applied E-field rather than the intensity.

Further investigations of the LLAP domain area for voltage delays up to 10 hours are shown in Fig. 4. However, for delay times beyond 700 s, the samples were kept in the dark before the application of the E-field, instead of being illuminated constantly by a broadband light source as in the short voltage delays experiments (< 700 s) which is likely to influence the relaxation rate of the space-charge distributions as will be discussed in Section 3. Additionally for longer time delays the inverted domains become fragmented, hence the measurements are increasingly inaccurate. Preferential nucleation was observed for time delays as long as 24 hours after laser irradiation, however the resulting domains were fragmented for the experimental conditions used. It is possible that higher laser intensities, higher E-fields, and/or longer exposures could produce solid domains as shown in Fig. 1 even for such long voltage delay times.

#113891 - $15.00 USD Received 7 Jul 2009; revised 20 Aug 2009; accepted 23 Aug 2009; published 1 Oct 2009
(C) 2009 OSA

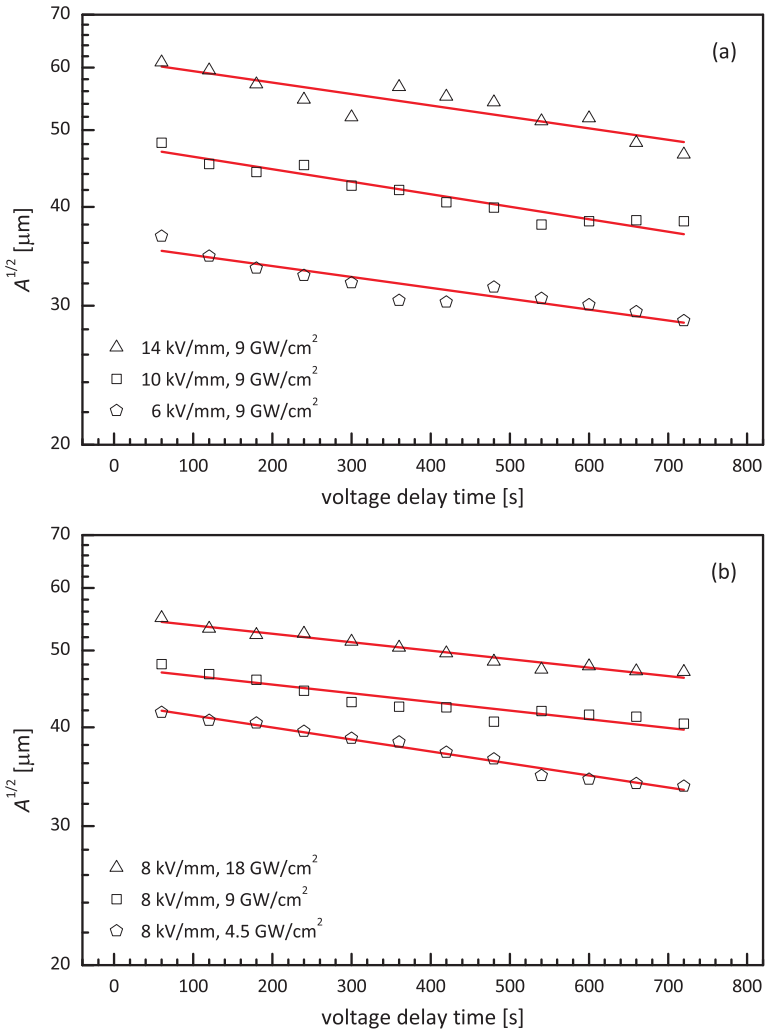

Fig. 2. Log-linear plots of the square root of the inverted LLAP domain areas, $A^{1/2}$, as a function of voltage delay time, measured from SEM images of HF-etched samples with conditions: (a) I = 9 GW/cm^2 and variable E-field amplitude; and (b) E = 8 kV/mm and variable laser intensity. The solid red lines represent single exponential decay function fits.

The fact that the inverted domain area reduces as a function of the time between the illumination event and the application of the E-field along with the independence of this decay rate (or time constant) on the experimental conditions (laser intensity, E-field value) suggests that the effect may be related to the relaxation of a space-charge distribution which has been formed as a result of the intense laser irradiation of the crystal. Photo-excited charge carriers in CLN can be electrons excited from impurity or defect energy levels to the conduction band, and electron-hole pairs excited directly across the band-gap via two-photon absorption [19] especially at high intensities. The driving force responsible for the migration of these photo-induced charges can be diffusion and/or the photovoltaic effect, resulting in a non-uniform space-charge distribution after illumination. The space-charge field produced by this space-charge distribution, if along the poling field, can contribute in a straightforward manner to the E_n reduction. Both the photovoltaic effect and diffusion can produce such space-charge distributions, with a component of space-charge field aligning along the poling field at –z face where domain nucleation occurs. The process of producing such a space-charge field by diffusion has been discussed in detail in Ref [7]. The photovoltaic case can be

#113891 - $15.00 USD Received 7 Jul 2009; revised 20 Aug 2009; accepted 23 Aug 2009; published 1 Oct 2009
(C) 2009 OSA

explained as follows: with the photovoltaic current flowing parallel to the spontaneous polarization, surface compensation charges are countered by photo-induced charges, leaving the dipoles at least partially uncompensated at the surface. The uncompensated depolarization field is oriented along the poling direction [16] and thus adds to the externally applied *E*-field, locally reducing the E_n. Additionally, photo-induced charges on the surface can screen the surface defects responsible for the domain nucleation [17], which might also contribute to the E_n reduction. After illumination, the photo-induced charges redistribute in the dark or under the influence of ambient light. The decay (redistribution) of the photo-induced space charges is thus reflected in the reduction of the inverted domain area as a function of the voltage time delay. All LLAP results which have been presented thus far correspond to experiments with undoped CLN crystals. No LLAP was observed for 5-mol% MgO-doped CLN (MgO:CLN) under these experimental conditions.

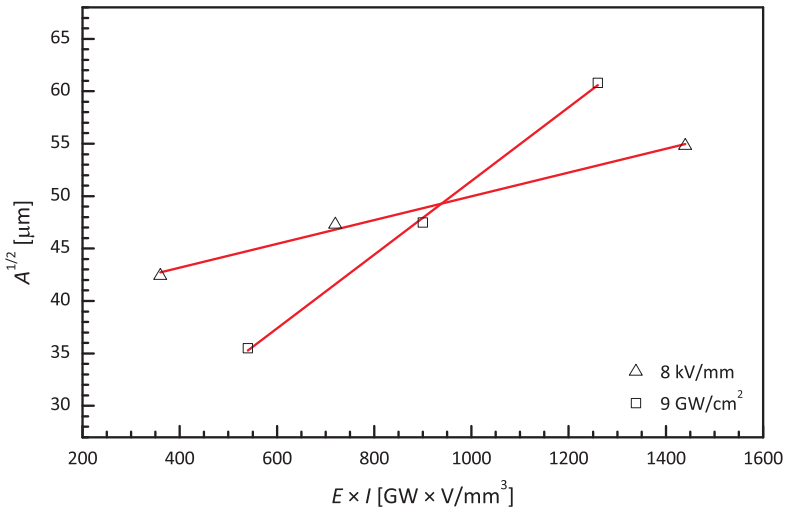

Fig. 3. Plot of the square root of the inverted LLAP domain area, $A^{1/2}$, versus the product of the applied external *E*-field and the intensity, $E \times I$, for a specific *E*-field (8 kV/mm) and a specific intensity (9 GW/cm^2). The solid red lines represent linear fits.

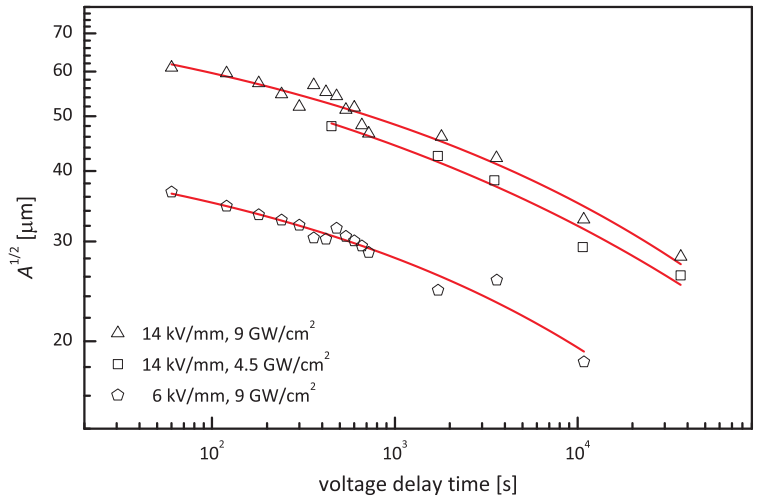

Fig. 4. Log plot of the square root of the inverted LLAP domain area, $A^{1/2}$, as a function of the voltage delay time for different laser intensities and *E*-fields. The solid red lines serve as a guide to the eyes.

#113891 - $15.00 USD Received 7 Jul 2009; revised 20 Aug 2009; accepted 23 Aug 2009; published 1 Oct 2009
(C) 2009 OSA

3. Photorefractive experiments and discussion

Single crystal LN is an electro-optic (EO) photoconductor and is known to exhibit photorefractive behavior [20] which can be enhanced in the visible spectral range by doping the crystal with iron for data storage applications [21]. Although the photorefractive effect is less pronounced in undoped crystals due to the lack of photo-excitable impurities, it is still present [22,23] and therefore can be used as a tool to study the dynamics of photo-induced space-charge distributions. Here we have recorded photorefractive gratings in undoped CLN crystals by two-beam-interference using the same laser source used for LLAP in order to study the dynamics of any space-charge fields that have been formed as a result of the ultrafast laser exposure and compare with the domain inversion dynamics in LLAP. The results of the photorefractive grating recording experiments provided a new insight to the effect of LLAP: a direct evaluation of the role of the space-charge distribution to the effect and also explaining a number of experimental observations such as the absence of latent effects in MgO-doped LN crystals and the much higher reduction of the E_n in MgO:CLN for LAP.

The experimental setup which was used for the recording of volume gratings in LN crystals is outlined in the schematic of Fig. 5. The original train of ultrafast laser pulses (400 nm, 150 fs) was divided into two parts by a cube beam splitter and the resulting beams were made to interfere in the LN crystal after propagating via the two distinct arms of a Michelson interferometer. For ultrashort pulse interference it is important to achieve both spatial and temporal overlap of the two pulses, hence the length of one arm of the interferometer was adjustable in order to achieve zero time delay. Monitoring of the grating recording and decay was achieved by measuring the diffracted power from a c.w. HeNe laser (λ_p = 633 nm) incident at the Bragg angle, as shown in Fig. 5. The diffracted signal exhibited strong sensitivity to the polarization of the probe beam, a fact that ensures that the grating is due to refractive index change as a result of the photorefractive (PR) effect and is not an absorption grating.

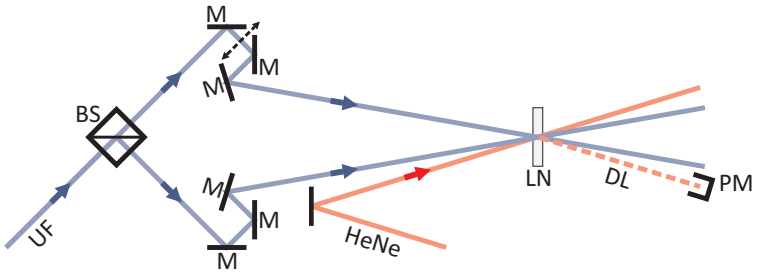

Fig. 5. Interferometric setup for recording and monitoring photorefractive gratings in LN using 150 fs ultrafast (UF) laser pulses at λ_r = 400 nm. The diffracted light (DL) of a c.w. HeNe laser at λ_p = 633 nm incident at the Bragg angle was used to monitor the grating recording/decay. M: mirror, BS: beam splitter, PM: optical power-meter. The period of the grating was ~1 μm. Spot diameters of the ultrafast and HeNe lasers are 1 and 0.8 mm respectively. The polarizations of both lasers were in the plane of the page (horizontal). The arrowed dash line indicates the variable arm of the interferometer.

The dynamic behavior (recording and decay) of PR gratings in both undoped CLN and 5-mol% MgO:CLN (Yamaju Ceramics Co., Ltd.) was investigated. The decay of the space-charge distribution in both crystals was monitored by measuring the power of the diffracted probe beam (λ_p = 633 nm) in the absence of the two recording beams (λ_r = 400 nm). The normalized temporal evolution of the square root of the diffraction efficiency, $\eta^{1/2}$, (which is proportional to the amplitude of the space charge field), is plotted as a function of time in Fig. 6a and Fig. 6b for undoped CLN and MgO:CLN, respectively. As the decay rate of the PR grating in both crystals was influenced by the intensity of the probe HeNe laser, we have

#113891 - $15.00 USD Received 7 Jul 2009; revised 20 Aug 2009; accepted 23 Aug 2009; published 1 Oct 2009
(C) 2009 OSA

obtained several decay curves corresponding to different values of the probe beam intensity as indicated in the graphs of Fig. 6.

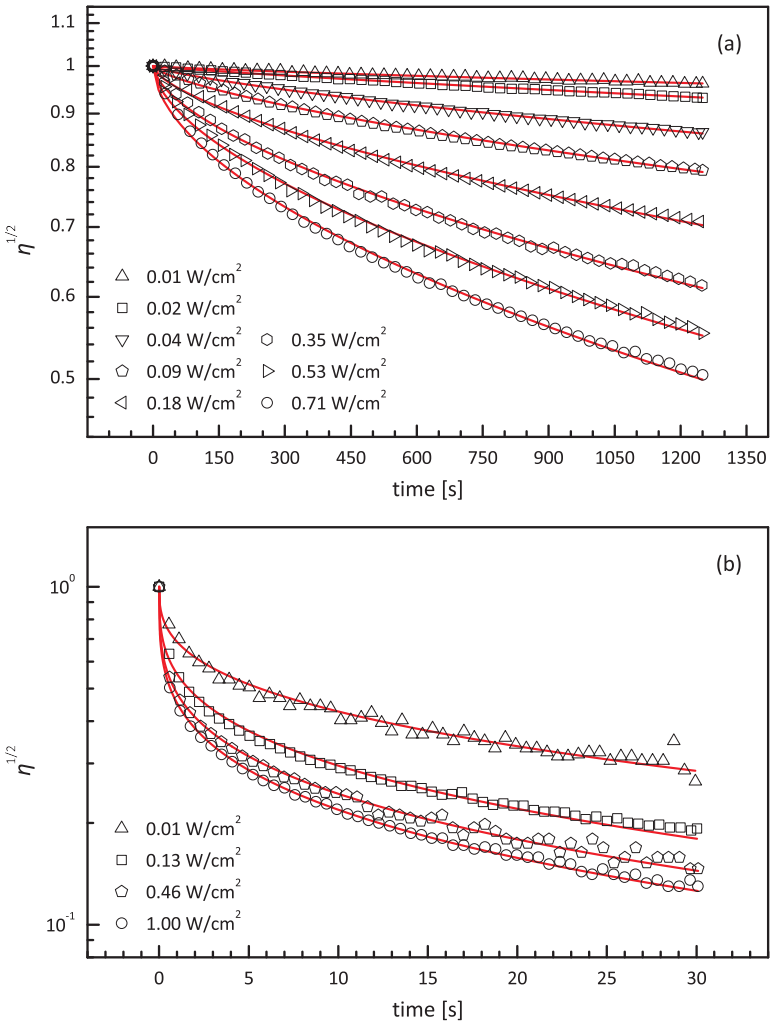

Fig. 6. Decays of the square root of the normalized PR grating diffraction efficiency, $\eta^{1/2}$, in (a) undoped CLN and (b) MgO:CLN for different probe laser intensities, I_p. The solid red curves correspond to stretched exponential decay fits.

We found that a stretched exponential decay curve described by the equation:

$$\eta^{1/2} = \exp\left[-(t/\tau)^{\beta}\right] \tag{3}$$

exhibits an improved fit as compared to a single exponential decay curve, where η is the normalized diffraction efficiency, t is the time, τ is the averaged relaxation time of the recorded hologram, and β is the stretch factor. The use of a stretched exponential function, also known as Kohlrausch-Williams-Watts function, is appropriate in our case as it describes a process that consists of a distribution of different relaxation processes [24]. The physical content of a stretched exponential decay of space charge distributions in undoped CLN has been described in [18,24] and is attributed to the large amount ($\approx 10^{20}$ cm^{-3}) of the intrinsic Nb_{Li} anti-site defects which exists in undoped CLN and provides an additional channel for the charge transport via hopping or tunnelling processes, apart from the conventional contribution

#113891 - $15.00 USD Received 7 Jul 2009; revised 20 Aug 2009; accepted 23 Aug 2009; published 1 Oct 2009
(C) 2009 OSA

of the conduction band [18]. From the stretched exponential fit, the decay time constant, τ, defined as the time in which the square root of the normalized diffraction efficiency reduces by a factor of e^{-1}, was derived for each probe HeNe laser intensity and the corresponding values are summarized in Table 2.

Table 2. Summary of the decay time constants τ, stretch factors β, decay rates τ^{-1}, and the relative reduction of the normalized PR grating diffraction efficiency $\Delta\eta^{1/2}$ from 60 s to 720 s, recorded in undoped CLN and MgO:CLN for different HeNe laser intensities I_p.

Crystal	I_p (W/cm^2)	τ (s)	β	τ^{-1} (s^{-1})	$\Delta\eta^{1/2}$
undoped CLN	0.71	2400	0.560	4.17×10^{-4}	0.318
	0.53	3040	0.581	3.29×10^{-4}	0.282
	0.35	4060	0.602	2.46×10^{-4}	0.239
	0.18	6370	0.640	1.57×10^{-4}	0.179
	0.088	10100	0.694	9.90×10^{-5}	0.123
	0.044	16600	0.734	6.01×10^{-5}	0.0802
	0.018	29600	0.841	3.38×10^{-5}	0.0378
	0.0088	81500	0.779	1.23×10^{-5}	0.0213
MgO:CLN	1.0	2.27	0.282	4.41×10^{-1}	
	0.46	3.01	0.287	3.32×10^{-1}	
	0.13	5.29	0.312	1.89×10^{-1}	
	0.013	15.8	0.355	6.34×10^{-2}	

Figure 7 shows a plot of the decay rate (τ^{-1}) as a function of the probe HeNe laser intensity. The main observation which can be made from the plot in Fig. 7 and Table 2 is that the photorefractive gratings in undoped CLN show a sufficiently slow decay, with time constants > 2400 s, thus a significant amount of the space-charge distribution should be present at the timescales where LLAP is observed. On the other hand, PR gratings in MgO:CLN decay three to four orders of magnitude faster than gratings recorded in undoped CLN, with time constants < 15.8 s, shorter than the smallest voltage time delay applied here which is 60 s, and this likely explains why LLAP was not observed for MgO:CLN crystals for these timescales. The fast decay of PR gratings in MgO:CLN is a consequence of the high dark conductivity of this material which is 4-5 orders of magnitude higher than undoped CLN according to e.g [25]. The dark conductivity of the crystal can be determined via [26]

$$\sigma_d = \varepsilon\varepsilon_0\tau_{I\approx 0}^{-1} \tag{4}$$

where ε = 28 is the dielectric constant of LN [27,28], ε_0 is the permittivity of free space and $\tau_{I\approx 0}$ is the decay time constant corresponding to a sufficiently low probe HeNe laser intensity, thus approaching the dark decay. The inverse of $\tau_{I\approx 0}$ can be estimated by substituting the lowest I_p values for undoped CLN and MgO:CLN in Table 2 which is ~0.01 W/cm^2. Figure 7 shows that at low HeNe laser intensity in the case of MgO:CLN, the τ^{-1} values are slow-decreasing hence the dark conductivity can be approximated by the conductivity at ~0.01 W/cm^2. However, for undoped CLN, τ^{-1} decreases quickly at low HeNe intensities, hence inducing a considerable uncertainty in estimating the value of dark conductivity. For this reason we conducted a grating decay experiment using a probe laser at a longer wavelength (800 nm), which did not affect the decay rate [22]. This measurement provided a value for the dark conductivity of undoped CLN which was very close to the value that corresponded to the HeNe intensity of I_p ~0.01 W/cm^2. According to Eq. (4), the corresponding dark conductivities were derived to be 1.57×10^{-11} $(\Omega\cdot m)^{-1}$ and 3.05×10^{-15} $(\Omega\cdot m)^{-1}$ for MgO:CLN and undoped CLN respectively, reconfirming the 4-5 orders of magnitude difference which has been reported in the literature [25].

To relate the PR grating decay to the delay time dependence of the inverted LLAP domain area, the relative reduction of the square root of the normalized PR grating diffraction efficiency, $\Delta\eta^{1/2}$, for the same time period in Fig. 2, from 60 s to 720 s, was derived from the stretched-exponential fitting for each HeNe laser intensity. The values of relative reduction are listed in Table 2 and plotted in Fig. 8. Comparing the relative reduction of the square root

#113891 - $15.00 USD Received 7 Jul 2009; revised 20 Aug 2009; accepted 23 Aug 2009; published 1 Oct 2009
(C) 2009 OSA

of the normalized PR grating diffraction efficiency, $\Delta\eta^{1/2}$, in that time period in undoped CLN with that of the square root of the inverted domain areas in LLAP, $\Delta A^{1/2}$, it is seen that the corresponding relative reduction for the domain length is larger than the corresponding ~dark PR grating decay. The range of the relative reduction for the square root of the inverted domain areas in Fig. 2 is indicated by the horizontal lines in Fig. 8 while the vertical lines indicate the corresponding range of probe HeNe laser intensities (0.13 – 0.28 W/cm^2). We believe that this is due to the fact that in the LLAP experiments the crystals were not kept in the dark but were continuously illuminated by a broadband light source (halogen bulb) for the in situ visualization of the poling process. The decay of the photo-induced space-charge distribution (hence the reduction of the inverted LLAP domain area with voltage delay time) should have been accelerated as a result of uniform illumination with radiation that contains a significant portion of short wavelength spectral components to which the crystal is more sensitive.

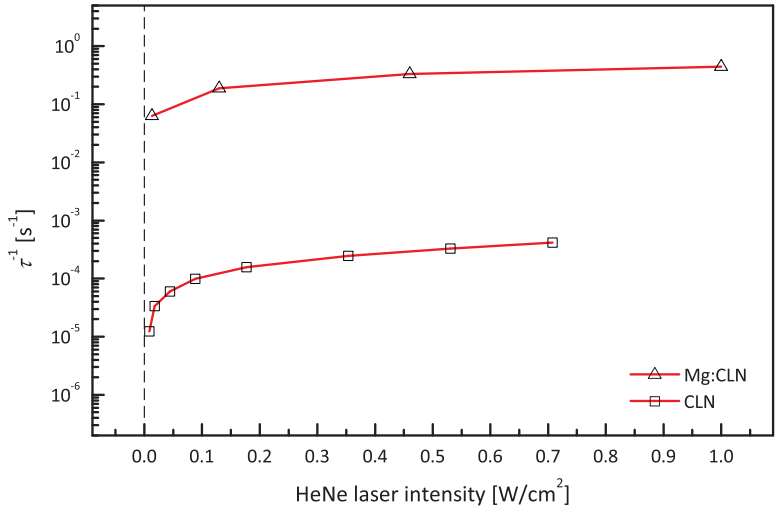

Fig. 7. Decay rate (τ^{-1}) as a function of the probe HeNe laser intensity for undoped CLN (squares) and MgO:CLN (triangles). The solid red curves are guides to the eyes.

The saturated diffraction efficiency of the PR gratings recorded in MgO:CLN was measured to be 1.5×10^{-4} which is one order of magnitude higher as compared to the corresponding saturated diffraction efficiency for undoped CLN crystals (1.3×10^{-5}) of the same thickness under identical recording and probing conditions. The diffraction efficiency of the grating was measured in real time during the recording of the grating with all three beams present simultaneously in the crystal. This difference in the diffraction efficiency corresponds to a 3.4 times larger amplitude of the space-charge field, and thus a 3.4 times larger amount of photo-induced charges being formed in MgO:CLN as compared to undoped CLN. This observation is of particular importance as it is in accordance with the much higher nucleation field reduction in MgO:CLN which is observed in LAP experiments [13].

Finally, the larger reduction of the E_n which was observed in LLAP for undoped CLN as compared with simultaneous LAP [29] cannot be explained with the data obtained here. However, it is possible that this further reduction in E_n can be associated with transient photo-excited charges [19] which screen the slowly evolving space-charge field in the presence of the ultrafast laser beam and which decay much faster than the LLAP observation times.

#113891 - $15.00 USD Received 7 Jul 2009; revised 20 Aug 2009; accepted 23 Aug 2009; published 1 Oct 2009
(C) 2009 OSA

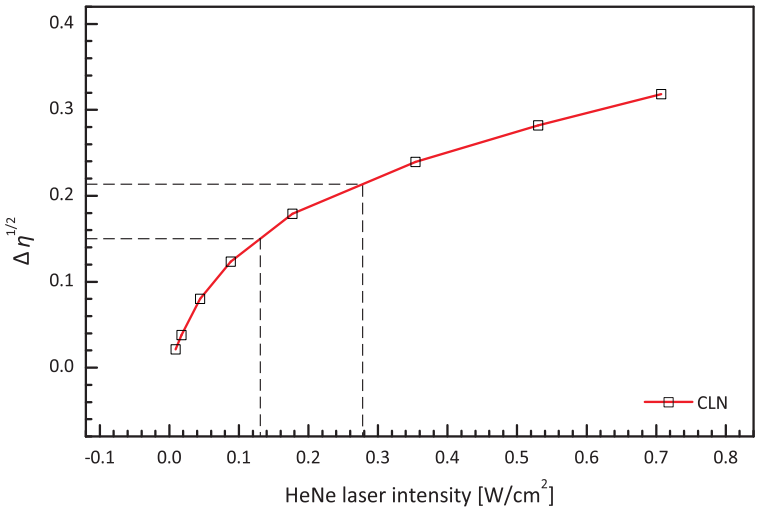

Fig. 8. Relative reduction of the square root of the normalized diffraction efficiency of the PR grating from 60 s to 720 s, $\Delta\eta^{1/2}$, as a function of HeNe laser intensity for undoped CLN. The solid red curve is a guide to the eyes. The range of the relative reduction of the square root of the inverted LLAP domain areas in Table 1, $\Delta A^{1/2}$, is indicated by the horizontal lines while the vertical lines indicate the corresponding range of HeNe laser intensities.

4. Conclusions

LLAP enables the de-coupling of the light illumination and application of the externally *E*-field, and has been demonstrated in undoped CLN. De-coupling these two steps can potentially improve the ferroelectric domain engineering process as it allows for independent design of each step. This includes the choice of illuminating wavelength and intensity to maximize the light-matter interaction, and choice of electrode materials for the optimization of the ferroelectric capacitor circuit for poling. Additionally, separation of the two processing steps can simplify the apparatus required, permitting the poling of thicker crystals or utilizing a larger area of the crystal by limiting surface leakage currents near the edges via the use of insulating oils (e.g. silicone oil). The size of the resulting inverted ferroelectric LLAP domains is a function of the time delay between the light illumination and the application of the *E*-field, which can be as long as ten hours. The dynamics of LLAP were attributed to the presence of a photo-induced space-charge distribution. The photorefractive effect in undoped CLN and MgO:CLN crystals was used as a tool for the monitoring of the dynamics of photo-induced space-charge distributions in these crystals. Good agreement between the relaxation dynamics of LLAP domain inversion and the PR grating was observed for undoped CLN, while the fast decay of the PR gratings observed in MgO:CLN explains the absence of the latent effect in this crystal. Finally the 10 × higher diffraction efficiency of PR gratings in MgO:CLN suggests a much larger amount of the photo-induced space charges in this crystal thus explaining the significant reduction of the nucleation field in this crystal during simultaneous light assisted poling (LAP).

Acknowledgements

The authors would like to acknowledge the financial contribution of the E.U. for funding this research in the framework of the STREP project “3D-DEMO”, the EPSRC Portfolio Partnership in Photonics (EP/C515668/1), and the Natural Sciences and Engineering Research Council of Canada (NSERC).

#113891 - $15.00 USD Received 7 Jul 2009; revised 20 Aug 2009; accepted 23 Aug 2009; published 1 Oct 2009
(C) 2009 OSA